Synthesis and Characterization of a New Family of Mixed Oxide−Proton Conductors Based on Tristrontium Oxysilicate

José M. Porras-Vázquez,[†] Enrique R. Losilla,[†] Laura León-Reina,[‡] María Martínez-Lara,[†] and Miguel A. G. Aranda*,[†]

Departamento de Química Inorgánica, Cristalografía y Mineralogía and Servicios Centrales de Investigación, Universidad de Málaga, 29071 Málaga, Spain

Received October 27, 2007. Revised Manuscript Received December 12, 2007

A new $Sr_3(Si_{1-x}Al_xO_4)O_{1-x/2}\square_{x/2}$ ($0.0 \le x \le 0.2$) oxysilicate series has been prepared, existing as a single phase for $x \le 0.11$. The evolution of the cell parameters was smooth along the series. The crystal structure of $Sr_3(Si_{0.9}Al_{0.1}O_4)O_{0.95}\square_{0.05}$ was determined from neutron powder diffraction data at room temperature. This compound crystallizes in the *P*4/*ncc* space group, $Z = 4$, with $a = 6.9427(1)$ Å, $c = 10.7992(1)$ Å, and $V = 520.53(1)$ Å^3. The Rietveld *R* values were $R_{WP} = 2.54\%$ and $R_F = 1.33\%$. The Si^{4+}/Al^{3+} aliovalent substitution is accompanied by oxygen vacancies for charge compensation. The crystal structure is described, as is a possible pathway for the "loosely bound" oxide anions that justifies the observed oxygen conductivity. Impedance data showed that the overall conductivity increased by more than 2 orders of magnitude from $Sr_3(SiO_4)O$ to $Sr_3(Si_{0.89}Al_{0.11}O_4)O_{0.945}\square_{0.055}$. Further electrochemical characterization under various atmospheres (dry air, wet air, dry 5% H_2 in Ar, and wet 5% H_2 in Ar) and impedance data as a function of the oxygen partial pressure indicated that there was a significant proton contribution to the overall conductivity. The oxide ion transference numbers, determined using a modified electromotive force method, ranged from 0.98 to 0.95 under strong reducing conditions. A large p-type electronic contribution was also observed for $Sr_3(Si_{0.89}Al_{0.11}O_4)O_{0.945}\square_{0.055}$ under oxidizing conditions, decreasing the oxide ion transference number to ~0.01 at 1173 K.

Introduction

Over the past three decades, solid oxide fuel cells (SOFCs) have been attracting considerable interest because of their potential utilization as alternative electrical power generation systems having small amounts of pollutant emission and high energy-conversion efficiencies.[1,2] Yttria-stabilized zirconia, YSZ, is the oxide-conducting electrolyte used in commercial systems because of its high oxide ion conductivity at elevated temperatures (1173–1273 K). However, there is great interest in the development of devices with lower operating temperatures to overcome side problems such as difficulties in cell sealing or short component lifetimes caused by the high operating temperature. On the other hand, high-temperature proton conductors are an important type of functional material because of their possible applications in electrochemical devices and membrane reactors, such as proton-conducting SOFCs, hydrogen sensors, steam electrolyzers, purification of hydrogen, and so on.[3]

There are two main approaches to developing new oxide-conducting materials. The first methodology is based on generating mobile vacancies in a given framework. There are many well-known examples of this approach, such as $Y_xZr_{2-x}O_{2-x/2}\square_{x/2}$ (YSZ), $Gd_xCe_{2-x}O_{2-x/2}\square_{x/2}$ (GDC), and $La_{1-x}Sr_xGa_{1-x}Mg_xO_{3-x}\square_x$ (LSGM). The second methodology is based on oxysilicates (or oxygermanates, oxyaluminates, etc.), in which "loosely bound" oxide anions (in some cases interstitial oxygen) are the charge carriers. Key examples of this second approach are oxygen-stoichiometric oxyapatite, $La_{9.33}\square_{0.67}(SiO_4)_6O_2$,[4] and oxymayenite, $[Ca_{12}Al_{14}O_{32}]O\square_5$.[5]

Following this second approach, we have recently reported a new family of complex oxide ion conductors based on tricalcium oxysilicate.[6,7] Ca_3SiO_5 is the main constituent of ordinary Portland cements, alite phase, and its formula is better written as $Ca_3(SiO_4)O$ in order to show its oxysilicate nature. The room-temperature (RT) structure of $Ca_3(SiO_4)O$ was determined from single-crystal data[8] to be triclinic, $P\bar{1}$, with $a = 11.67$ Å, $b = 14.24$ Å, $c = 13.72$ Å, $\alpha = 105.5°$, $\beta = 94.33°$, $\gamma = 90°$, and $V/Z = 121.68$ Å^3. This phase contains some oxide anions that are bonded only to the

* To whom correspondence should be addressed. E-mail: g_aranda@uma.es. Tel: +34 952131874. Fax: +34 952132000.
[†] Departamento de Química Inorgánica, Cristalografía y Mineralogía.
[‡] Servicios Centrales de Investigación.

(1) Steele, B. C. H.; Heinzel, A. *Nature* **2001**, *414*, 345.
(2) Ormerod, R. M. *Chem. Soc. Rev.* **2003**, *32*, 17.
(3) Iwahara, H.; Asakura, Y.; Katahira, K.; Masahiro, T. *Solid State Ionics* **2004**, *168*, 299.
(4) (a) Nakayama, S.; Kageyama, T.; Aono, H.; Sadaoka, Y. *J. Mater. Chem.* **1995**, *5*, 1801. (b) Kendrick, E.; Islam, M. S.; Slater, P. R. *J. Mater. Chem.* **2007**, *17*, 3104. (c) León-Reina, L.; Losilla, E. R.; Martínez-Lara, M.; Bruque, S.; Aranda, M. A. G. *J. Mater. Chem.* **2004**, *14*, 1142. (d) León-Reina, L.; Losilla, E. R.; Martínez-Lara, M.; Bruque, S.; Llobet, A.; Sheptyakov, D. V.; Aranda, M. A. G. *J. Mater. Chem.* **2005**, *15*, 2489.
(5) (a) Lacerda, M.; Irvine, J.T. S.; Glasser, F. P.; West, A. R. *Nature* **1988**, *332*, 525. (b) Palacios, L.; de la Torre, A. G.; Bruque, S.; Garcia-Muñoz, J. L.; Garcia-Granda, S.; Sheptyakov, D.; Aranda, M. A. G. *Inorg. Chem.* **2007**, *46*, 4167. (c) Boysen, H.; Lerch, M.; Stys, A.; Senyshyn, A. *Acta Crystallogr., Sect. B* **2007**, *63*, 675.
(6) Porras-Vázquez, J. M.; de la Torre, A. G.; Marrero-López, D.; Losilla, E. R.; Aranda, M. A. G. *Dalton Trans.* **2006**, 2691.
(7) Porras-Vázquez, J. M.; de la Torre, A. G.; Losilla, E. R.; Aranda, M. A. G. *Solid State Ionics* **2007**, *178*, 1073.
(8) Golovastikov, N. I.; Matveeva, R. G.; Belov, N. V. *Sov. Phys. Crystallogr.* **1975**, *20*, 441.

10.1021/cm703079d CCC: $40.75
Published on Web 01/23/2008

calcium atoms and form rows that are the responsible for the oxide conductivity properties.[6] Tricalcium silicate also shows a small p-type electronic contribution under oxidizing conditions [the oxide ion transference numbers (t_o) ranged from 0.97 to 0.89 in going from reducing (dry 5% H_2-Ar/air gradient) to oxidizing (O_2/air gradient) conditions at 1023 K] and displays an important proton contribution under a humidified atmosphere. Studies of the possibility of aluminum substitution at the tetrahedral site[7] showed that oxygen vacancies cannot be stabilized by partial substitution of silicon with aluminum, since the $Ca_3(Si_{1-x}Al_xO_4)O_{1-x/2}\square_{x/2}$ series is not formed. The aluminum doping in this system is achieved by substitution at both calcium and silicon sites, yielding a series with fixed oxygen content: $Ca_{3-x/2}Al_{x/2}(Si_{1-x/2}Al_{x/2}O_4)O$ ($0.0 \le x \le 0.03$).[7] Electrochemical characterization indicated that these compounds are oxide anion conductors that have a small contribution of p-type electronic conductivity ($t_o \approx 0.98$ and 0.91 under dry 5% H_2-Ar/air and dry O_2/air gradients, respectively) and also show a very important proton contribution to the overall conductivity under wet atmospheres, even at high temperatures. It must be noted that the proton transference number (t_H) measured in a steam concentration cell was 0.55 at 1023 K.

On the other hand, tristrontium oxysilicate was first prepared by Nurse,[9] who reported its optical and X-ray powder data. Single-crystal X-ray data showed that Sr_3SiO_5 is tetragonal (space group *P*4/*ncc*, $a = 6.934$ Å, $c = 10.72$ Å, $V/Z = 128.85$ Å^3), but only an approximate crystal structure was deduced from symmetry and packing considerations.[10] This compound, whose formula can also be written as $Sr_3(SiO_4)O$ in order to show its oxysilicate nature, contains oxide anions that are weakly bonded to the strontium atoms and form rows that may display oxide conductivity properties similar to those of $Ca_3(SiO_4)O$ derivatives. Despite differences in unit cells and symmetries, $Sr_3(SiO_4)O$ and $Ca_3(SiO_4)O$ are based on similar structural units: M^{2+} ions (M = Ca, Sr), O^{2-} ions, and isolated SiO_4^{4-} tetrahedra. Furthermore, their crystal structures are related.[11] In both frameworks, all of the oxide ions are surrounded by regular M^{2+} octahedra; the difference between the structures has to do with the way the SiO_4^{4-} tetrahedra are packed.[11] Tristrontium oxysilicate was studied decades ago by cement chemists[10,11] because of its relationship to alite, the main component of Portland cement. Since that time, however, little additional information has been reported; to the best of our knowledge, the literature contains only a few reports concerning its thermodynamic stability[12] and photoluminescence properties.[13–15]

The aim of this work was to evaluate tristrontium oxysilicate-based materials as candidates for oxide ion conductors, since the reported structure of $Sr_3(SiO_4)O$ was compatible with fast oxide ion diffusion. To accomplish this, we have prepared stoichiometric $Sr_3(SiO_4)O$ and three related series: $Sr_3(Si_{1-x}M_xO_4)O_{1-x/2}\square_{x/2}$ (M = Al, Ga), which have variable oxygen content, and $Sr_{3-x/2}Al_{x/2}(Si_{1-x/2}Al_{x/2}O_4)O$, which has fixed oxygen content. In this way, it was possible to analyze the roles of oxygen vacancies and Al^{3+} substitution in the ionic conductivity properties. Room-temperature neutron powder diffraction (RT-NPD) and high-resolution laboratory X-ray powder diffraction (LXRPD) were used to determine the crystal structures. Electrochemical characterization allowed us to establish the nature of the conductivity, highlighting the contributions of the oxide and proton charge carriers.

Experimental Section

Synthesis. Three oxysilicate series have been prepared: $Sr_3(Si_{1-x}Al_xO_4)O_{1-x/2}\square_{x/2}$ ($0.0 \le x \le 0.2$), $Sr_3(Si_{1-x}Ga_xO_4)O_{1-x/2}\square_{x/2}$ ($0.0 \le x \le 0.09$), and $Sr_{3-x/2}Al_{x/2}(Si_{1-x/2}Al_{x/2}O_4)O$ ($x = 0.06, 0.10$). These compounds were synthesized with conventional ceramic methods using high-purity oxides and carbonates as starting materials: SiO_2 (ABCR, quartz powder, 99.3%), γ-Al_2O_3 (Alfa, 99.997%), Ga_2O_3 (Alfa, 99.99%), and $SrCO_3$ (Alfa, 99.99%). Strontium carbonate was precalcined at 1673 K for 15 h in order to achieve decarbonation. Stoichiometric amounts of the reagents were mixed in an agate mortar for 15 min, then ground in a Fritsch ball mill (model Pulverisette 7, a 45 cm^3 agate vessel containing 7 agate balls with diameters of 15 mm) for 30 min at 200 rpm with reverse rotation each 5 min, and finally heated at 1273 K for 6 h; this procedure yielded ~3 g of each sample according to the following overall reactions:

$$3SrCO_3 + (1-x)SiO_2 + (x/2)M_2O_3 \xrightarrow{\Delta} Sr_3(Si_{1-x}M_xO_4)O_{1-x/2}\square_{x/2} + 3CO_2$$

$$(3-x/2)SrCO_3 + (1-x/2)SiO_2 + (x/2)Al_2O_3 \xrightarrow{\Delta} Sr_{3-x/2}Al_{x/2}(Si_{1-x/2}Al_{x/2}O_4)O + (3-x/2)CO_2$$

where, in the former reaction, M = Al or Ga.

The resulting powders were reground in a planetary ball mill, pelletized at 65 MPa (giving diameters of 20 mm and thicknesses of 3 mm), and heated in air for various temperatures and times: (1) Aluminum samples were calcined at 1773 K for 6 h and then reground, pelletized, and heated at 1873 K for an additional 6 h. (2) Gallium pellets were covered with powder of the same material (to avoid/minimize gallium losses) and heated at 1573–1773 K for 18 h two times with intermediate regrindings. The samples are hereafter labeled as Sr_3M_x for the series $Sr_3(Si_{1-x}M_xO_4)O_{1-x/2}\square_{x/2}$ (M = Al, Ga). The compounds $Sr_{3-x/2}Al_{x/2}(Si_{1-x/2}Al_{x/2}O_4)O$ ($x = 0.06, 0.10$) were not single-phase, as discussed below.

Powder Diffraction. All compounds were characterized by LXRPD at room temperature. The powder patterns were collected on an X'Pert Pro MPD automated diffractometer equipped with a Ge(111) primary monochromator (strictly monochromatic Cu $K\alpha_1$ radiation) and an X'Celerator detector. The overall measurement time was ~4 h per pattern in order to obtain very good statistics over the 2θ range of 5–145° with a step size of 0.017°. All Rietveld analyses[16] were carried out by using the GSAS suite of programs.[17]

(9) Nurse, R. W. *J. Appl. Chem.* **1952**, *2*, 244.
(10) Glasser, L. S. D.; Glasser, F. P. *Acta Crystallogr.* **1965**, *18*, 453.
(11) Glasser, L. S. D. *Acta Crystallogr.* **1965**, *18*, 455.
(12) (a) Rög, G.; Langanke, B.; Borchardt, G.; Schmalzried, H. *J. Chem. Thermodyn.* **1974**, *6*, 1113. (b) Matveev, G. M.; El'kin, G. B. *Theor. Found. Chem. Eng.* **1992**, *26*, 759.
(13) (a) Park, J. K.; Kim, C. H.; Park, S. H.; Park, H. D.; Choi, S. Y. *Appl. Phys. Lett.* **2004**, *84*, 1647. (b) Park, J. K.; Choi, K. J.; Yeon, J. H.; Lee, S. J.; Kim, C. H. *Appl. Phys. Lett.* **2006**, *88*, 043511.
(14) Jee, S. D.; Park, J. K.; Lee, S. H. *J. Mater. Sci.* **2006**, *41*, 3139.
(15) Jang, H. S.; Jeon, D. Y. *Appl. Phys. Lett.* **2007**, *90*, 041906.
(16) Rietveld, H. M. *J. Appl. Crystallogr.* **1969**, *2*, 65.

RT-NPD patterns were collected on an HRPT diffractometer[18] (using the SINQ neutron source at Paul Scherrer Institut, Villigen, Switzerland) for $Sr_3(Si_{0.9}Al_{0.1}O_4)O_{0.95}\square_{0.05}$ in a vanadium can. The neutron wavelength, ~1.15 Å, was selected by the 511 reflection of the vertically focusing Ge monochromator. The overall measurement time was 6 h per pattern in order to obtain good statistics over the 2θ range of 8–145° (8.27–0.6 Å) with a step size of 0.05°.

Microstructural Characterization. The morphologies of the sintered pellets were studied using a JEOL SM 840 scanning electron microscope. The surfaces were polished with diamond spray (3 and 1 μm) and thermally etched at 50 K below the sintering temperature for 45 min. Finally, the samples were metallized by gold sputtering for better image definition.

Sintering Conditions and Conductivity Measurements. Electrical characterization was performed on cylindrical pellets (having diameters of ~5 mm and thicknesses of ~1 mm) obtained by pressing ~0.1 g of sample at 1000 MPa for 2 min. The pellets were sintered at a heating rate of 10 K min^{-1} to different temperatures depending on composition: aluminum samples were calcined at 1923 K for 6 h and gallium samples at 1573–1773 K for 6 h. As before, the Ga pellets were covered with powder of the same material to avoid gallium losses. Electrodes were made by coating opposite pellet faces with METALOR 6082 platinum paste and then heating to 1323 K at a rate of 10 K min^{-1} for 15 min in air in order to decompose the paste and harden the Pt residue. Successive treatments were performed in order to achieve an electrical resistance of less than 1 Ω on each pellet face.

Impedance spectroscopy data were collected in two different flowing atmospheres (dry and wet synthetic air) using an HP4284A impedance analyzer over the frequency range from 20 Hz to 1 MHz with an applied voltage of 1 V. Electrical measurements were taken on heating and cooling in the 673–1273 K temperature range every 50 ± 1 K at 10 K min^{-1} with a delay time of 45 min at each temperature to ensure thermal stabilization. Measurements were electronically controlled by the winDETA package of programs.[19]

High-temperature conductivity measurements as a function of oxygen partial pressure [$p(O_2)$, from its pressure in air to $\sim 10^{-20}$ atm] were performed in a closed tube-furnace cell. The $p(O_2)$ values were monitored using a YSZ oxygen sensor placed next to the pellet in the cell. The conductivity was continuously recorded as a function of $p(O_2)$. The process consisted of flushing the system with a dry gas mixture of 5% H_2 in Ar for 12 h at 973, 1073, and 1173 K in order to reach a minimum in oxygen activity inside the furnace and ensure that the sample was close to the equilibrium under those conditions. Next, the flushing was switched off, and the oxygen partial pressure was allowed to slowly recover to atmospheric pressure by free diffusion, since the system was not fully airtight. Each isothermal cycle took more than 72 h to complete.

Oxide ion transference numbers were determined by a modified electromotive force (emf) method that took electrode polarization into account.[20,21] This modification of the classical emf technique eliminated possible errors in the determination of ion transference numbers arising from electrode polarization. These errors are not negligible for electrolyte materials, which have relatively low electronic conductivities.[21,22] The values of t_o were measured under a $p(O_2)$ gradient of pure O_2/air and dry 5% H_2-Ar/air, using a continuous flux of these gases in the 923–1173 K temperature range. A YSZ tube was used to measure the theoretical emf (E_{th}) under these conditions. The emf observed in the sample (E_{obs}) was measured using an external variable resistance (R_M) connected in parallel with the measuring cell and varying from 1500 Ω to 100 kΩ. Experimental data were fitted with the equivalent circuit (eq 1) as proposed by Gorelov.[20] In this case, the ionic resistance (R_o), the electronic resistance (R_e), and the polarization resistance (R_η) are related to E_{th} and E_{obs} according to the equation

$$\frac{E_{th}}{E_{obs}} - 1 = (R_o + R_\eta)\left[\frac{1}{R_e} + \frac{1}{R_M}\right] \qquad (1)$$

Equation 1 indicates that a plot of $(E_{th}/E_{obs} - 1)$ versus $1/R_M$ should be linear with a slope equal to $(R_o + R_\eta)$ and a $(E_{th}/E_{obs} - 1)$-axis intercept equal to $(R_o + R_\eta)/R_e$. The total resistance (R_T) was determined independently by impedance spectroscopy. The oxide ion transference numbers were calculated from the equation $t_o = 1 - R_T/R_e$.

Results and Discussion

Synthesis, Single-Phase Existence Ranges, and Chemical Stability. The series $Sr_3(Si_{1-x}Al_xO_4)O_{1-x/2}\square_{x/2}$ ($0.0 \le x \le 0.2$) was obtained by solid-state reaction in the form of highly crystalline compounds (see Figure 1). The dominant phase under our synthetic conditions was invariably the tristrontium oxysilicate type of structure. Two secondary phases, Sr_2SiO_4 (PDF 88–271) and $Sr_4Al_2O_7$ (PDF 28–1204), were observed for $x \ge 0.15$. Analysis of the LXRPD patterns using the Rietveld method showed that the $Sr_3Al_{0.15}$ and $Sr_3Al_{0.20}$ samples contained 12.5(2) and 11.1(3) wt % Sr_2SiO_4, respectively (see Table 1). The intensities of $Sr_4Al_2O_7$ reflections increased with Al content; however, the crystal structure of $Sr_4Al_2O_7$ has not been reported, and therefore, it was not possible to quantify its content using the Rietveld method. In any case, the compositional limit of the Sr_3Al_x series must be close to $x = 0.11$ under the reported synthetic conditions.

On the other hand, the synthesis of the series $Sr_3(Si_{1-x}Ga_xO_4)O_{1-x/2}\square_{x/2}$ ($0.0 \le x \le 0.09$) was optimized by studying the heating temperatures and times. At very high temperatures, volatilization of Ga_2O_3 occurred, and the samples became dark blue (typical of Ga_2O), likely as a result of partial reduction of Ga(III) to Ga(I) catalyzed by the platinum crucible. To overcome these drawbacks, two different respective strategies were simultaneously employed: first, the temperature was lowered from 1873 to 1573 K as the gallium content increased from $x = 0.0$ to $x = 0.09$; and second, the pellets were fully buried within powder of the same composition. Although this methodology yielded white pellets, the samples had low thermal stabilities, and prolonged heatings at temperatures higher than those used in the syntheses produced dark pellets and segregation of Sr_2SiO_4 and SrO. Because of these limitations, an exhaustive study of the single-phase existence range was not undertaken. For

(17) Larson, A. C.; von Dreele, R. B. *GSAS program*, Report No. LA-UR-86748; Los Alamos National Laboratory: Los Alamos, NM, 1994.
(18) Fischer, P.; Frey, G.; Koch, M.; Konnecke, M.; Pomjakushin, V.; Schefer, J.; Thut, R.; Schlumpf, N.; Burge, R.; Greuter, U.; Bondt, S.; Berruyer, E. *Phys. B* **2000**, *146*, 276.
(19) *winDETA*; Novocontrol GmbH: Hundsangen, Germany, 1995.
(20) Gorelov, V. P. *Elektrokhimiya* **1988**, *24*, 1380.
(21) Marozau, I. P.; Marrero-López, D.; Shaula, A. L.; Kharton, V. V.; Tsipis, E.; Núñez, P.; Frade, J. *Electrochim. Acta* **2004**, *49*, 3517.
(22) Kharton, V. V.; Viskup, A. P.; Figueiredo, F. M.; Naumovich, E. N.; Yaremchenko, A. A.; Marques, F. M. B. *Electrochim. Acta* **2001**, *46*, 2879.

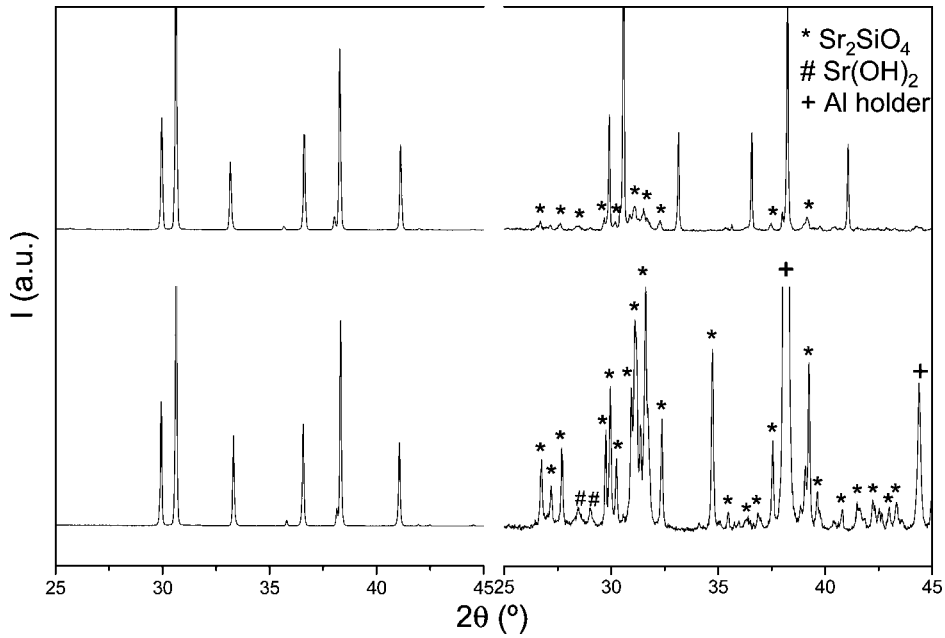

Figure 1. LXRPD patterns ($\lambda = 1.5406$ Å) for $Sr_3(SiO_4)O$ (bottom) and $Sr_3(Si_{0.89}Al_{0.11}O_4)O_{0.945}\square_{0.055}$ (top). In each panel, the pattern on the left corresponds to the compound prepared by solid-state reaction, while the pattern on the right, which shows partial decomposition, corresponds to the sample heated at 773 K for 12 h under a constant flux of steam [$p(H_2O) = 2.34$ kPa].

Table 1. Unit Cell Parameters and Rietveld Disagreement Factors for the $Sr_3(Si_{1-x}Al_xO_4)O_{1-x/2}\square_{x/2}$, $Sr_{3-x/2}Al_{x/2}(Si_{1-x/2}Al_{x/2}O_4)O$, and $Sr_3(Si_{1-x}Ga_xO_4)O_{1-x/2}\square_{x/2}$ Series at Room Temperature

compound	a (Å)	c (Å)	V/Z (Å^3)	R_{WP} (%)	R_F (%)	% Sr_2SiO_4
$Sr_3(SiO_4)O$[a]	6.9513(1)	10.7611(1)	129.998(2)	9.85	2.09	−
$Sr_3(Si_{0.97}Al_{0.03}O_4)O_{0.985}\square_{0.015}$[a]	6.9487(1)	10.7728(1)	130.039(2)	10.35	2.33	−
$Sr_3(Si_{0.93}Al_{0.07}O_4)O_{0.965}\square_{0.035}$[a]	6.9450(1)	10.7894(1)	130.101(1)	9.25	3.18	−
$Sr_3(Si_{0.9}Al_{0.10}O_4)O_{0.95}\square_{0.05}$[b]	6.9426(1)	10.7988(1)	130.138(1)	2.54	1.33	−
$Sr_3(Si_{0.89}Al_{0.11}O_4)O_{0.945}\square_{0.055}$[a]	6.9416(1)	10.8053(1)	130.165(2)	10.17	3.83	−
$Sr_3(Si_{0.85}Al_{0.15}O_4)O_{0.925}\square_{0.075}$[a]	6.9418(1)	10.8080(1)	130.205(1)	9.93	3.48	12.5(2)
$Sr_3(Si_{0.80}Al_{0.20}O_4)O_{0.90}\square_{0.10}$[a]	6.9426(1)	10.8099(1)	130.258(1)	12.14	3.69	11.1(3)
$Sr_{2.97}Al_{0.03}(Si_{0.97}Al_{0.03}O_4)O$	6.9463(1)	10.7867(1)	130.117(1)	8.69	2.43	12.7(2)
$Sr_{2.95}Al_{0.05}(Si_{0.95}Al_{0.05}O_4)O$	6.9490(1)	10.7948(1)	130.128(1)	9.83	3.08	17.7(3)
$Sr_3(Si_{0.97}Ga_{0.03}O_4)O_{0.985}\square_{0.015}$[a]	6.9517(1)	10.7803(1)	130.244(2)	7.54	1.68	3.3(1)
$Sr_3(Si_{0.91}Ga_{0.09}O_4)O_{0.955}\square_{0.045}$[a]	6.9513(1)	10.8063(1)	130.542(2)	9.78	1.89	0.9(1)

[a] LXRPD data refinement. [b] Joint LXRPD and NPD data refinement at RT.

the sake of comparison with the aluminum series, two samples, $Sr_3Ga_{0.03}$ and $Sr_3Ga_{0.09}$, were studied using LXRPD and impedance spectroscopy.

The unit cell parameters derived from Rietveld refinements for stoichiometric $Sr_3(SiO_4)O$ and the Sr_3Al_x and Sr_3Ga_x compounds are given in Table 1. First, it can be seen that the overall trend within each series was an increase in volume with increasing metal content. This behavior was expected because M^{3+} cations (M = Al, Ga) have larger ionic radii[23] than Si^{4+}. Second, the unit cell edges of the gallium derivatives were larger than those of the corresponding aluminum compounds, as expected because Ga^{3+} has a larger ionic radius[23] than Al^{3+}.

The stabilities of the Sr_3M_x series (M = Al, Ga) were studied under different atmospheres and temperatures. The samples did not undergo degradation under a constant flow of 5% H_2-Ar or O_2 over the temperature range from 1173 K to RT. To study the stability of these phases under moist conditions, the samples were heated under a constant flux of steam [$p(H_2O) = 2.34$ kPa] at different temperatures. In the high-temperature range (1273–800 K), LXRPD patterns of the resulting samples did not show evidence of decomposition; however, below 773 K, the samples decomposed into Sr_2SiO_4 and $Sr(OH)_2$ (see Figure 1). It must be highlighted that the degree of decomposition depended on the aluminum content; samples containing larger amounts of aluminum were more resistant to degradation, as shown by the right-hand patterns in Figure 1. All of the experimental results indicated that the aluminum/gallium strontium oxysilicate-based materials have good chemical stability above 800 K.

All attempts to synthesize the $Sr_{3-x/2}Al_{x/2}(Si_{1-x/2}Al_{x/2}O_4)O$ series in single-phase form by solid-state reaction were unsuccessful. As x increased, larger amounts of Sr_2SiO_4 and $Sr_4Al_2O_7$ phases appeared in the patterns (see Table 1). The unit cell volumes of the samples with nominal composition $Sr_{3-x/2}Al_{x/2}(Si_{1-x/2}Al_{x/2}O_4)O$ ($x = 0.06, 0.10$) were larger than that of $Sr_3(SiO_4)O$. However, a smaller unit cell was

(23) Shannon, R. D. *Acta Crystallogr., Sect. A* **1976**, *32*, 751.

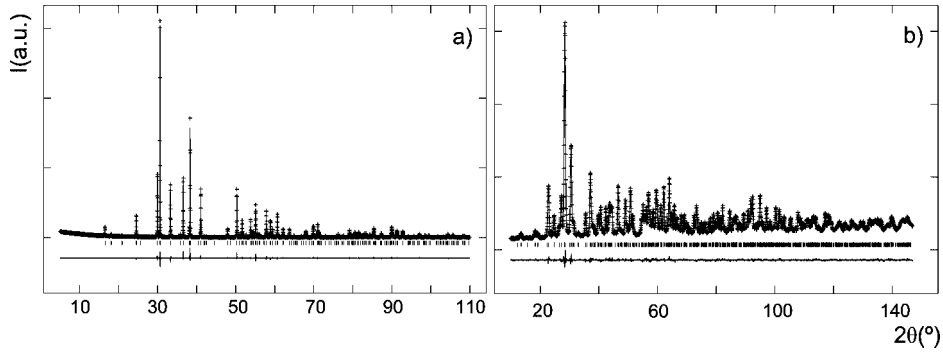

Figure 2. Observed (crosses), calculated (solid line), and difference (bottom) RT powder diffraction patterns: (a) laboratory X-ray powder data ($\lambda = 1.5406$ Å) for $Sr_3(SiO_4)O$; (b) neutron powder data ($\lambda = 1.154$ Å) for $Sr_3(Si_{0.9}Al_{0.1}O_4)O_{0.95}\square_{0.05}$.

expected. Although the Al^{3+} ionic radius is larger than that of Si^{4+}, it is much smaller than that of Sr^{2+}. It is worth pointing out that the unit cell volumes of the $Ca_{3-x/2}Al_{x/2}(Si_{1-x/2}Al_{x/2}O_4)O$ series were smaller than that of $Ca_3(SiO_4)O$.[7] Hence, it is clear that aluminum was incorporated into the framework but replaced only the silicate units in $Sr_3(SiO_4)O$; there was no evidence to support the partial substitution of strontium by aluminum. As a result, this series was not characterized further. It can be speculated that the different behaviors of the $Ca_{3-x/2}Al_{x/2}(Si_{1-x/2}Al_{x/2}O_4)O$ series, which exists, and the $Sr_{3-x/2}Al_{x/2}(Si_{1-x/2}Al_{x/2}O_4)O$ series, which does not appear to be stable, may be a consequence of the fact that the difference of the ionic radii for Sr^{2+} and Al^{3+} is much larger than that for Ca^{2+} and Al^{3+}.

Crystal Structures. In addition to the unit cell parameters reported in Table 1, the crystal structures of $Sr_3(SiO_4)O$ and $Sr_3(Si_{0.9}Al_{0.1}O_4)O_{0.95}\square_{0.05}$ were studied in detail. $Sr_3(SiO_4)O$ was analyzed by high-resolution X-ray powder diffraction to confirm the approximate structure reported in 1965.[10] $Sr_3Al_{0.1}$ was studied with NPD mainly in order to confirm the presence of oxide vacancies in the loosely bound oxide sublattice. Powder diffraction patterns were analyzed by the Rietveld method with the GSAS software package[17] using a pseudo-Voigt peak-shape function with the asymmetry correction included. The following overall parameters were refined: background coefficients, cell parameters, zero-shift error, peak shape parameters, and phase fractions (if necessary). The fits were very good, and the Rietveld plots for $Sr_3(SiO_4)O$ and $Sr_3(Si_{0.9}Al_{0.1}O_4)O_{0.95}\square_{0.05}$, respectively, are shown in Figure 2a,b. The final unit cell parameters and R values for $Sr_3(SiO_4)O$ and $Sr_3(Si_{0.9}Al_{0.1}O_4)O_{0.95}\square_{0.05}$ are given in Table 1, and the final atomic parameters are given in Table 2. It must be noted that the occupation factors for Si, Al, and O were refined but also constrained in order to maintain the electroneutrality of the refined structural formula: the variation of the occupation factor for O2 was half of that for the Si/Al ratio. The anisotropic atomic displacement parameters can be found in the deposited CIF files (see the Supporting Information).

The atomic parameters for $Sr_3(SiO_4)O$ (see Table 2) were similar to those reported previously[10] but had smaller errors. The main conclusion obtained from the structural study of $Sr_3(Si_{0.9}Al_{0.1}O_4)O_{0.95}\square_{0.05}$ was the confirmation of partial substitution of Al at the Si site with the concomitant introduction of oxide vacancies (see Table 2). However, the refined occupation factor of 4(1)% for aluminum was smaller than the nominal value of 10%. This may have been due to the presence of an amorphous strontium aluminate phase (as there was no secondary crystalline phase) and/or inaccuracies in the Rietveld refinement. Taken together, the variation of the unit cell parameters (see Table 1) and the Si/Al occupation factors (see Table 2) establish the existence of the $Sr_3(Si_{1-x}Al_xO_4)O_{1-x/2}\square_{x/2}$ solid solution in the composition range $0 \le x \le 0.11$.

Table 2. Atomic Parameters for $Sr_3(SiO_4)O$ and $Sr_3(Si_{0.9}Al_{0.1}O_4)O_{0.95}\square_{0.05}$ Derived from Rietveld Refinements in Space Group *P4/ncc*

parameter	$Sr_3(SiO_4)O$	$Sr_3Al_{0.1}$
Sr1, 8f, (x, y, $^3/_4$)		
x	0.4376(1)	0.4354(1)
y	0.9376(1)	0.9354(1)
$U_{iso} \times 100$ (Å^2)	0.55	0.72
Sr2, 4c, ($^1/_4$, $^1/_4$, z)		
z	−0.0085(1)	−0.0076(2)
$U_{iso} \times 100$ (Å^2)	0.88	1.30
Si/Al, 4b, ($^1/_4$, $^3/_4$, 0)		
$U_{iso} \times 100$ (Å^2)	0.10	0.54
occupation factor (Si/Al)	1.00/−	0.96(1)/0.04(1)
O1, 16 g, (x, y, z)		
x	0.4053(5)	0.4045(1)
y	0.6453(5)	0.6443(1)
z	0.5911(3)	0.5926(1)
$U_{iso} \times 100$ (Å^2)	0.66	1.34
O2, 4c, ($^1/_4$, $^1/_4$, z)		
z	0.2248(6)	0.2257(1)
$U_{iso} \times 100$ (Å^2)	0.19	0.94
occupation factor	1.00	0.980(5)

The crystal structure of $Sr_3(SiO_4)O$ is depicted in Figure 3. The packing of SiO_4 tetrahedra along the c axis is clearly seen in the left panel of Figure 3. This figure also shows the alternating packing of O2 and Sr2 along the c axis, which would not allow oxide diffusion. However, there is a pathway between the loosely bound oxide anions (O2) along the diagonal of the ab plane, as highlighted with the double arrow in Figure 3. This pathway can be clearly seen in the right panel of Figure 3, where the O2 anions are directly packed. Diffusion of O2 along the highlighted direction is impeded by the presence of two Sr1 cations. The key structural parameter is the Sr1···Sr1 distance between the O2 anions, highlighted with the dotted line in Figure 3. This distance is 3.69 and 3.64 Å in $Sr_3Al_{0.0}$ and $Sr_3Al_{0.1}$, respectively.

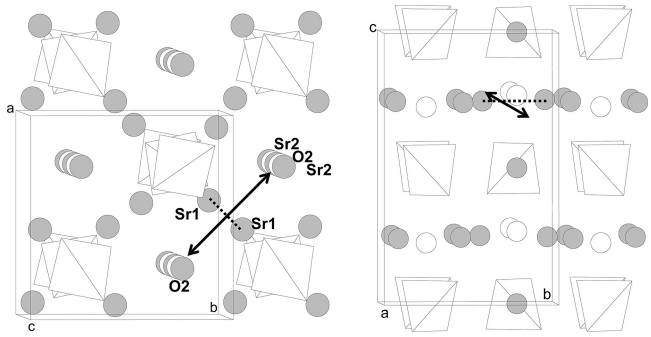

Figure 3. Crystal structure of $Sr_3(SiO_4)O$, with the SiO_4 groups shown as tetrahedra and strontium cations and oxide anions displayed as shaded and white spheres, respectively. (left) Projection close to the *ab* plane. (right) Projection close to the *cb* plane. The significance of the double arrow and the dotted line in each panel is explained in the text.

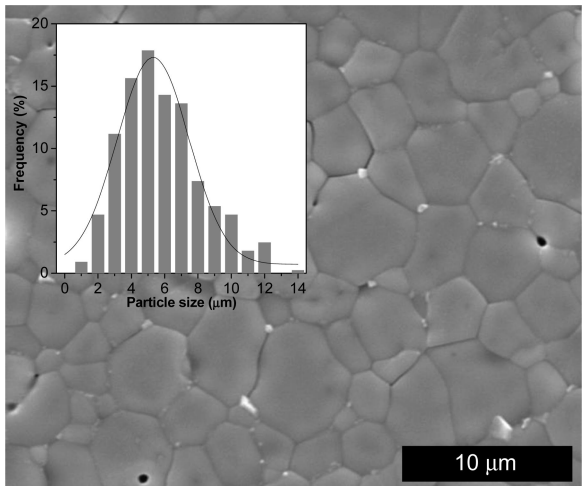

Figure 4. SEM micrograph of the polished and thermally etched surface of a $Sr_3(Si_{0.89}Al_{0.11}O_4)O_{0.945}\square_{0.055}$ pellet sintered for 6 h at 1923 K. The inset shows the grain size distribution plot.

Electrical Characterization. *a. Sintering Conditions and High-Temperature Conductivity Behavior.* The sintering conditions for the pellets of the Sr_3Al_x series at 1923 K led to dense specimens with compactions ranging from 88% ($x = 0.0$) to 96% ($x = 0.11$) of the theoretical value (taking into account the pellet mass and volume and the crystallographic density). Figure 4 shows an SEM micrograph obtained for a sintered $Sr_3Al_{0.11}$ pellet as a representative of the series. The pellet had low porosity and no indications of liquid phase formation or phase segregation at the grain boundaries. Additionally, no contamination due to the ball-milling process was detected in the sintered pellets. The SEM micrographs were analyzed to evaluate both the grain size distribution (see the inset of Figure 4) and the corresponding average grain size. The microstructure showed Gaussian distributions, and the average grain size did not change with increasing aluminum content (i.e., the average grain sizes for $Sr_3Al_{0.0}$ and $Sr_3Al_{0.11}$ were 6.0 and 5.5 μm, respectively). On the other hand, the limited thermal stability range for $Sr_3Ga_{0.03}$ and $Sr_3Ga_{0.09}$ samples resulted in pellets with higher porosities. The pellet densities were ∼85% at the highest possible sintering temperatures (1773 and 1573 K for $x = 0.03$ and 0.09, respectively).

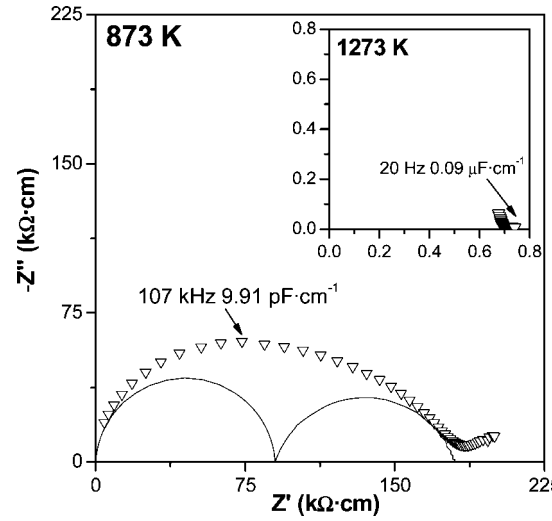

Figure 5. Plot of the complex impedance plane for $Sr_3(Si_{0.89}Al_{0.11}O_4)O_{0.945}\square_{0.055}$ at 873 K (1273 K in the inset) under dry air.

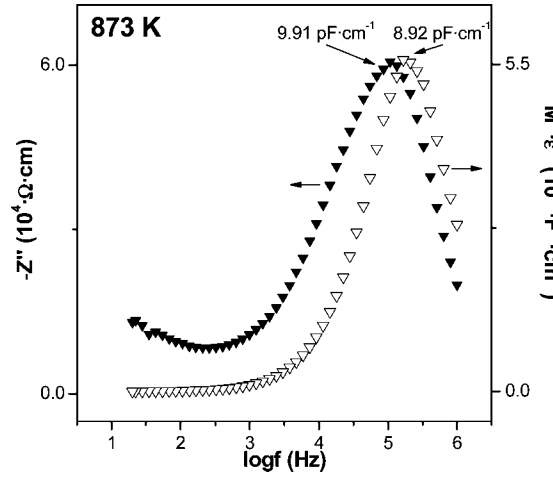

Figure 6. Spectroscopic plots at 873 K of $-Z''$ (▼) and M'' (▽) as a function of log f for $Sr_3(Si_{0.89}Al_{0.11}O_4)O_{0.945}\square_{0.055}$.

Some results from the $Sr_3Al_{0.11}$ impedance study, which were typical for the series, are shown in Figures 5 and 6. The plot of the complex impedance plane for $Sr_3Al_{0.11}$ (Figure 5) shows a broad arc at 873 K, of which at least two components could be distinguished. The set of semicircles indicates that two different contributions, likely due to the grain interior (bulk) and to internal interfaces (grain boundary and porosity), were present. Lower-frequency processes were observed at high temperature in the form of a spike, with an associated capacitance of ∼0.1 μF cm^{-1} at 20 Hz and 1273 K (see the Figure 5 inset). From these data, it may be concluded that the samples showed ionic conductivity, as previously reported for related tricalcium oxysilicate-based materials.[6,7]

To investigate the electrical microstructure of the pellets, it was useful to analyze the spectroscopic plots (plots of $-Z''$ and M'' vs log f) for the same impedance data, since this analysis could reveal whether the overall pellet resistance represented the bulk resistance of the grains or was influenced by grain-boundary effects. The maxima of the spectroscopic plots for $Sr_3Al_{0.11}$ (Figure 6) were quite close (separated by less than 1 order of magnitude in frequency), indicating that

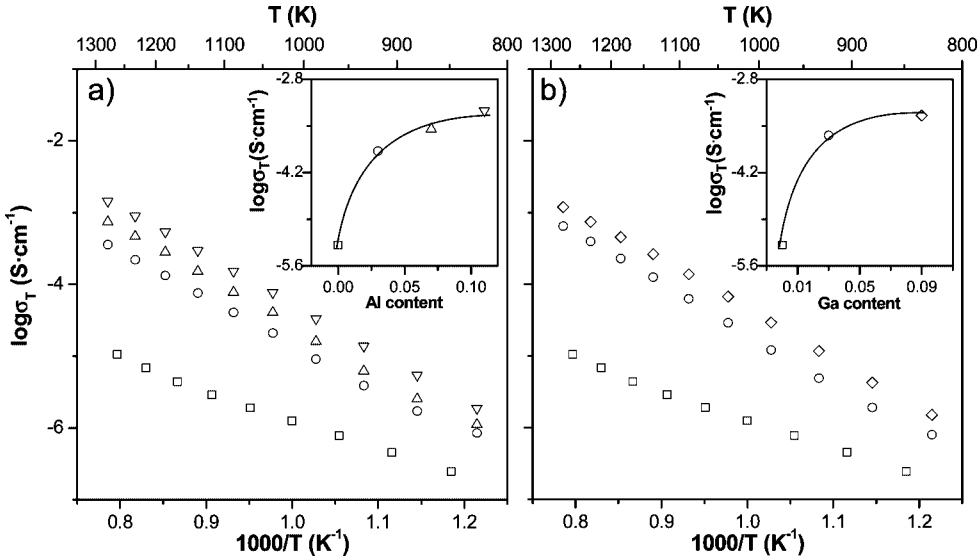

Figure 7. Arrhenius plots of log σ_T for (a) $Sr_3(Si_{1-x}Al_xO_4)O_{1-x/2}\square_{x/2}$ [$x = 0.0$ (□), 0.03 (○), 0.07 (△), and 0.11 ()] and (b) $Sr_3(Si_{1-x}Ga_xO_4)O_{1-x/2}\square_{x/2}$ [$x = 0.0$ (□), 0.03 (○), and 0.09 (◇)] under dry air. The insets show the variation of the overall conductivity as a function of metal content at 1173 K (the lines are guides to the eyes).

the impedance peak was associated with the same RC element that was responsible for the modulus peak. However, the associated capacitances (~9 pF cm^{-1} for M″ and 10 pF cm^{-1} for Z″) were somewhat larger than expected for a homogeneous bulk value (~2 pF cm^{-1} would be expected, assuming a typical high-frequency permittivity ϵ' of 10–20). To further examine this point, we plotted the real part of the complex capacitance as a function of frequency (not shown). At low frequencies, the blocking electrode effect could be seen, and at higher frequencies, the curves showed a clear relaxation from ~10 pF toward lower values (in the picofarad range) with increasing frequency. The relaxation at ~10 pF can be attributed to a very thick grain boundary or constriction resistance in the region of the grain−grain contacts observed in the SEM micrograph (Figure 4). This component dominated the Z″ spectrum and represented the main part of the total resistance of the samples.

Overall pellet conductivities (σ_T) were obtained from the Z′-axis intercepts of the spikes and/or the low-frequency ends of the arcs and are given in Figure 7 in the traditional Arrhenius representation. These plots of overall conductivities fall on a set of straight lines without large discontinuities between compositions. For the Sr_3Al_x series (Figure 7a), the calculated activation energies ranged from 1.02(3) to 1.30(1) eV; for the Sr_3Ga_x series (Figure 7b), the corresponding range was 1.02(3)–1.35(1) eV.

The variations of the total conductivities with metal (Al or Ga) content under static dry air at 1173 K for the Sr_3Al_x and Sr_3Ga_x series are given in the insets of Figure 7a,b. The total conductivity values increased with Al/Ga content, likely reaching a maximum for the highest aluminum/gallium-loaded materials. The total conductivity values at 1173 K were 5.12×10^{-6}, 1.32×10^{-4}, 2.80×10^{-4}, and 5.37×10^{-4} S cm^{-1} for the $Sr_3Al_{0.0}$, $Sr_3Al_{0.03}$, $Sr_3Al_{0.07}$, and $Sr_3Al_{0.11}$ samples, respectively, and 2.28×10^{-4} and 4.53×10^{-4} S cm^{-1} for the $Sr_3Ga_{0.03}$ and $Sr_3Ga_{0.09}$ compositions, respectively. The conductivity value for $Sr_3Al_{0.0}$ was slightly lower than that reported[7] for Ca_3Si (1.53×10^{-5} S cm^{-1}) at the same temperature, although the electrical microstructure and porosity of the two samples were quite similar. This behavior was likely a consequence of the different crystal structures of the two compounds.

Aluminum/gallium doping yielded a very significant enhancement in the overall electrical conductivity (2 orders of magnitude) for the two strontium oxysilicate series. As a first approximation, σ_T increased with increases in the amounts of oxide vacancies and the unit cell volumes (see Table 1). The activation energies of the conduction process also increased upon metal doping. This was likely due to the smaller bottlenecks (Sr1···Sr1 distances) in the doped systems, as described in the previous section. However, this increase may also indicate the presence of some sort of additional association enthalpy term, probably due to clustering of oxygen vacancies. Electron microscopy studies designed to develop a proper understanding of the local structure are underway and will be reported elsewhere.

The $p(O_2)$ dependence of total conductivity was studied by performing isothermal oxidation runs from the low $p(O_2)$ value associated with the 5% H_2-Ar atmosphere to the high $p(O_2)$ value in air at temperatures between 973 and 1173 K. Conductivity data for $Sr_3Al_{0.11}$ and $Sr_3Al_{0.0}$ as a function of $p(O_2)$ are shown in Figure 8. The total conductivities measured at $p(O_2) = 0.23$ atm and 1173 K in this study were 5.6×10^{-4} and 4.0×10^{-6} S cm^{-1} for $Sr_3Al_{0.11}$ and $Sr_3Al_{0.0}$, respectively. The total conductivities measured under air at 1173 K in the impedance study were 5.4×10^{-4} and 5.1×10^{-6} S cm^{-1} for $Sr_3Al_{0.11}$ and $Sr_3Al_{0.0}$, respectively. We underline that these numbers were not identical because they were obtained using different cells. However, there was relatively good agreement between the two data sets. It must be noted that the materials did not degradate under very reducing conditions, as the LXRPD patterns of the final samples were identical to those of the pristine materials.

Several conclusions were drawn from the variable-$p(O_2)$ study. First, there was p-type electronic behavior at relatively

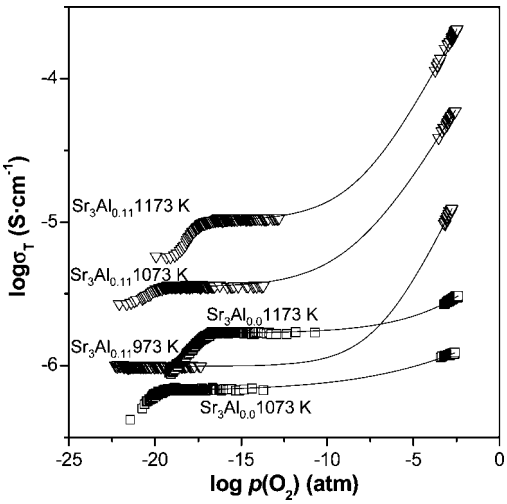

Figure 8. Overall conductivity data versus oxygen partial pressure for $Sr_3(Si_{0.89}Al_{0.11}O_4)O_{0.945}\square_{0.055}$ and $Sr_3(SiO_4)O$ at the labeled temperatures. The lines correspond to the ideal behavior described by the equation $\sigma_T = \sigma_{ion} + \sigma_p^o\, p(O_2)^{1/4}$.

high oxygen partial pressures. The contribution of the p-type electronic conductivity (σ_p^o) was evaluated by fitting the experimental data to eq 2:

$$\sigma_T = \sigma_{ion} + \sigma_p^o p(O_2)^{1/4} \qquad (2)$$

The fits (shown as solid lines in Figure 8) gave p-type electronic conductivity values of 5.5×10^{-4}, 1.3×10^{-4}, and 4.2×10^{-5} S cm^{-1} at 1173, 1073, and 973 K, respectively, for $Sr_3Al_{0.11}$ at $p(O_2) = 0.23$ atm; similar calculations for $Sr_3Al_{0.0}$ yielded 2.2×10^{-6} and 6.9×10^{-7} S cm^{-1} at 1173 and 1073 K, respectively. From the plots given in Figure 8, it is clear that the p-type electronic contribution was much larger for $Sr_3Al_{0.11}$ than for $Sr_3Al_{0.0}$. Second, the ionic plateau values at intermediate oxygen partial pressures indicated that the ionic conductivity for $Sr_3Al_{0.11}$ was about 1 order of magnitude larger than that of $Sr_3Al_{0.0}$. Therefore, the increase of 2 orders of magnitude in the overall conductivity under air determined in the impedance spectroscopy study was due to an increase in both the electronic and ionic conductivities. Third, there was also a drop in conductivity at very low $p(O_2)$ (reducing conditions). This type of drop in conductivity at very low oxygen partial pressures has been reported previously for other oxide electrolytes, i.e., pyrochlore-structured $La_2Zr_2O_7$,[24] perovskite-structured $SrZrO_3$- and $BaCeO_3$-based materials,[25–28] and Ca_3SiO_5-type materials.[6,7] This effect was interpreted in terms of a decrease in the proton contribution as the oxygen partial pressure decreases.[26] It must be highlighted that decreasing the oxygen partial pressure induces a decrease in the water partial pressure. Finally, it must be remarked that the lowest $p(O_2)$ value reached was not low enough to isolate the pure oxide contribution from total mixed ionic (oxide−proton) conductivity for $Sr_3Al_{0.0}$. Additional work using an electrochemical pump to obtain very low oxygen partial pressures in order to measure pure oxide conductivities with a negligible proton contribution is underway.

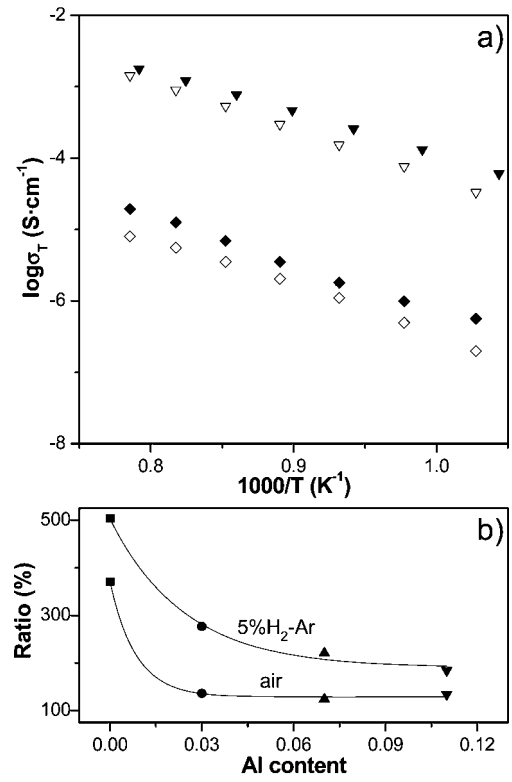

Figure 9. (a) Arrhenius plots of log σ_T for $Sr_3(Si_{0.89}Al_{0.11}O_4)O_{0.945}\square_{0.055}$ under dry (open symbols) and wet (solid symbols) atmospheres: synthetic air (triangles) and 5% H_2-Ar (diamonds). (b) Wet-to-dry conductivity increase [$100\% \times (\sigma_{wet} - \sigma_{dry})/\sigma_{dry}$] for all members of the Sr_3Al_x series at 973 K under two different atmospheres: air and 5% H_2-Ar.

Finally, oxide transport numbers for $Sr_3Al_{0.11}$ at 1173 K could be estimated, as a plateau in the conductivity ($\sigma_o = 5.8 \times 10^{-6}$ S cm^{-1}) at very low oxygen partial pressures was observed, indicating nearly pure oxide conductivity. Therefore, the ratio between the conductivities at very low oxygen partial pressures and close to open atmosphere (oxide, proton, and p-type conductivities) suggested an oxide ion transference number close to 0.01 at $p(O_2) = 0.23$ atm.

b. Mixed Ionic (Oxide−Proton) Conductivity. In order to establish the existence of mixed oxide−proton conductivity in the Sr_3Al_x series, an impedance spectroscopy study under various atmospheres was carried out. Figure 9 a shows Arrhenius plots of total conductivities for $Sr_3Al_{0.11}$ under constant flows of dry air, wet air, dry 5% H_2-Ar, and wet 5% H_2-Ar atmospheres. It is clear from that figure that the sample had the highest conductivity under wet air and the lowest conductivity under dry 5% H_2-Ar; moreover, the conductivities under wet atmospheres were always slightly higher than those under dry conditions for all temperatures. The reduction of the resistivity through an increase in the water partial pressure confirmed the existence of a proton contribution to the overall conductivity in this system. This result was in agreement with the conductivity versus $p(O_2)$ study, where a conductivity decrease at very low oxygen partial pressures was observed. Furthermore, the proton conductivity remained even at very high temperatures.

(24) Labrincha, J. A.; Frade, J. R.; Marques, F. M. B. *Solid State Ionics* **1997**, *99*, 33.
(25) Labrincha, J. A.; Frade, J. R.; Marques, F. M. B. *Solid State Ionics* **1993**, *61*, 71.
(26) Labrincha, J. A.; Marques, F. M. B.; Frade, J. R. *J. Mater. Sci.* **1995**, *77*, 2785.
(27) Yamija, T.; Susuki, H.; Yogo, T.; Iwahara, H. *Solid State Ionics* **1992**, *51*, 101.
(28) Iwahara, H.; Uchida, H.; Ono, K.; Ogaki, K. *J. Electrochem. Soc.* **1988**, *135*, 529.

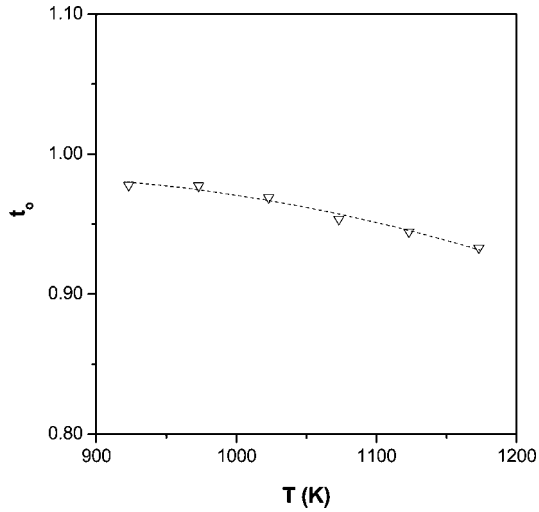

Figure 10. Temperature dependence of the oxide ion transference number (t_o) for $Sr_3(Si_{0.89}Al_{0.11}O_4)O_{0.945}\square_{0.055}$ under a reducing (dry 5% H_2-Ar/air gradient) atmosphere.

The activation energies for $Sr_3Al_{0.11}$ decreased from 1.32(1) eV under dry air to 1.17(1) eV under wet air. Similar behavior was observed for dry and wet 5% H_2-Ar atmospheres, for which the activation energies were 1.31(5) and 1.22(5) eV, respectively. The activation energies were smaller for samples containing less aluminum. For instance, the $Sr_3Al_{0.0}$ activation energy decreased from 1.02(3) to 0.66(2) eV in going from dry to wet air and from 1.46(4) to 0.61(6) eV in going from dry to wet 5% H_2-Ar. Typical activation energies for mixed oxide−proton conductors range between 0.5 and 1.0 eV. Figure 8b shows the conductivity increases $[100\% \times (\sigma_{wet} - \sigma_{dry})/\sigma_{dry}]$ for all members of the Sr_3Al_x series under air and 5% H_2-Ar atmospheres at 973 K. This figure indicates that the proton contribution was more important (yielding up to a 5-fold increase) when the number of vacancies decreased to zero. The proton conductivity contribution decreased with aluminum content as the electronic contribution increased, as discussed in the next section.

c. Electron–Hole Conductivity. Figure 10 plots the oxide ion transference number as a function of temperature for $Sr_3Al_{0.11}$. The values of t_o showed a slight decrease (from 0.98 at 923 K to 0.93 at 1173 K) under a dry 5% H_2-Ar/air gradient. It must be noted that one face of the pellet was subjected to air and thus was susceptible to p-type conductivity as described above. The slight decrease in t_o with increasing temperature was ascribed to a larger p-type electronic contribution. This may have been associated with oxygen absorption from the air by the sample, according to the following electrochemical reaction:

$$\tfrac{1}{2}O_2 + V_O^{\bullet\bullet} \leftrightarrow O_o^x + 2h^{\bullet} \quad (3)$$

where $V_O^{\bullet\bullet}$ and O_o^x are vacant and oxygen sites in the lattice, respectively, and $h^{\bullet}$ is a hole, in the Kröger−Vink notation.[29] This oxygen intercalation process increases the concentrations of interstitial oxygen and holes, both of which are mobile charge carriers. Therefore, the increase in aluminum content in the $Sr_3(Si_{1-x}Al_xO_4)O_{1-x/2}\square_{x/2}$ series increased the number of oxide vacancies and thus, from eq 3, the number of holes. Increasing the aluminum content also increased the hole mobility, as the average jump distance between holes decreased. Both effects point toward higher p-type electronic conductivity with increasing x.

Conclusions

The series of compounds $Sr_3(Si_{1-x}Al_xO_4)O_{1-x/2}\square_{x/2}$ ($0.0 \leq x \leq 0.11$) are oxide conductors at high temperature; similar oxide conductivity was previously reported for the related materials $Ca_{3-x/2}Al_{x/2}(Si_{1-x/2}Al_{x/2}O_4)O$.[6,7] $Sr_3(Si_{0.89}Al_{0.11}O_4)O_{0.955}\square_{0.055}$ had an overall conductivity that was 2 orders of magnitude larger than that of the pristine compound, $Sr_3(SiO_4)O$. This increase was due to larger oxide and p-type electronic contributions. Proton conductivity was also measured, and it was significant in the temperature range studied. For $Sr_3(Si_{0.89}Al_{0.11}O_4)O_{0.955}\square_{0.055}$, the oxide ion transference numbers ranged from 0.98 to 0.95 for very low oxygen partial pressures. Electrochemical analysis showed that the p-type electronic contribution under oxidizing conditions was very important and that the oxide ion transference number was as low as 0.01 at 1173 K under air.

Acknowledgment. Financial support from the Ministry of Education and Science (MEC) of Spain (Research Grant MAT2007-07483-C2-1) is acknowledged. This work was partially performed at the spallation neutron source SINQ at the Paul Scherrer Institut, Villigen, Switzerland. J.M.P.-V. thanks MEC for a studentship.

Supporting Information Available: Crystallographic information files for $Sr_3(SiO_4)O$ and $Sr_3(Si_{0.9}Al_{0.1}O_4)O_{0.95}\square_{0.05}$ (CIF). This material is available free of charge via the Internet at http://pubs.acs.org.

CM703079D

(29) Kröger, F. A.; Vink, H. J. *Solid State Phys.* **1956**, *3*, 307.